Composition and optical properties of chromium oxynitride films

Jin Wang, Yuchun Tu, Yanyan Yuan, Han Qian, Philippe Jonnard, Rui Lan

Composition and optical properties of chromium oxynitride films

Jin Wang[1], Yuchun Tu[2], Yanyan Yuan[1*], Han Qian[1],

Philippe Jonnard[3], Rui Lan[1]

[1] School of Materials Science and Engineering, Jiangsu University of Science and Technology, No.666 Zhaohui Road, Zhenjiang, Jiangsu Province, 212100, China

[2] Shanghai Institute of Laser Plasma, No.1129, Chenjiashan road, Jiading district, Shanghai, 201800, China

[3] Sorbonne Université, Faculté des Sciences et Ingénierie, UMR CNRS, Laboratoire de Chimie Physique-Matière et Rayonnement, 4 place Jussieu, F-75252Paris cedex 05, France

Abstract

The films with various components were prepared by using the reaction gases N_2 and O_2 combined with the Cr_2O_3 and CrN targets. The focus of this study is at the composition, optical, and bandgap properties of the CrO_xN_y thin films. X-ray diffraction, X-ray photoelectron spectroscopy and UV-vis-NIR spectroscopy were used to investigate the phase structure, chemical composition and optical properties of the films, respectively. The results show that the films mainly consisted of CrO_2 phases. The (O+N)/Cr atomic ratio deduced from XPS in the films prepared with the Cr_2O_3 target increased with the increase of nitrogen flow, while the nitrogen concentration in samples prepared with the CrN target was greatly affected by O_2 gases flow. When the oxygen flow was as low as 1.0 sccm, the sample mainly composed of oxides. The thin films prepared with the oxide target presented a good transmittance of 60~80% in the visible range. The bandgap, as obtained using the absorption value, spaned a range of 1.3-2.6 eV. These results provide an excellent suggestion for the preparation of the chromium oxynitrides films applied in the aspect of mechanical, optical and electrical properties.

Keywords：chromium oxynitride film; optical properties; bandgap; composition

*Corresponding author：yuan.yanyan@just.edu.cn

1. Introduction

Transition metal oxynitrides have potential technological applications due to their diversity of properties with respect to metal oxides and nitrides [1]. Transition-metal nitrides, such as ZrN, CrN, and TiN, as refractory compounds, possess exceptional physical properties, including high hardness, high melting point, good chemical stability, as well as corrosion resistance [2]. On the other hand, transition metal oxides have excellent chemical stability, high refraction index, high resistance and dielectric constant, which were widely used in the field of optical and electrical devices [3-8]. Zheng *et al.* pointed out that a CrO_x layer added into the organic-inorganic halide perovskite solar cells greatly improved the stability of the electron transport layer in the air and also the conversion efficiency [9]. Ternary, quaternary, and multicomponent films were prepared by adding other high-melting point materials, which have excellent performance, for example high hardness, chemical stability, corrosion resistance, and so on [10-13].

Transition-metal oxynitrides were considered as mixtures of transition-metal nitrides and oxides phases instead of single phase. Thus, they possessed both the hardness of oxides and toughness of nitrides. Balancing the oxide/nitride ratio allowed us to tune the bandgap and crystallographic order between oxides and nitrides, and hence to meet the requirements of mechanical, optical, and electrical properties, such as in TiO_xN_y [14-16], ZrO_xN_y [17-19], TaO_xN_y [20, 21] thin films. The potential properties such as high chemical stability, wear resistance, corrosion resistance and optical properties of the chromium oxide films have attracted wide attention.

To obtain films with adjustable performance between that of the chromium oxide and the chromium nitride films, the preparation of the chromium oxynitride films was performed by adding a small amount of oxygen to chromium nitrides or adding a small amount of nitrogen to chromium oxides. Due to the possible change of the nitrogen/oxygen ratio, chromium oxynitride films were widely used for their electrical, optical and mechanical properties, as well as chemical stability [22, 23]. Commonly, chromium oxynitride thin films were regarded as a mixture of CrN_x and CrO_x, not as a single-phase chromium oxynitride compound [24]. Depending on its stoichiometry, A CrN_x exhibits metal-like properties ($\rho \approx 6.4\times10^{-4}\,\Omega\cdot\mathrm{cm}$ $x\approx0.93$) or semiconductor properties ($\rho>1\times10^{-2}\,\Omega\cdot\mathrm{cm}$, $x\approx1.06$), while

CrO_x is an insulating material (E_g=4 eV, ρ_{Cr2O3}>>1 $\Omega \cdot cm$) [25]. Arvinte *et al.* reported a CrO_xN_y film prepared by adding a small amount of oxygen to the transition metal nitride, and the change in the nitrogen/oxygen atomic ratio tuned the bandgap value in a wide range, so that the properties of the film were changed between metal-like and semiconductor-like [26]. Rawal *et al.* reported the fabrication of the chromium oxynitride films and the titanium oxynitride nanofilms by radio frequency (RF) reactive magnetron sputtering using metal Cr and Ti targets in a helium atmosphere along with O_2 and N_2 as reactive gases. The variation in the bandgap was observed for both systems [27]. Mientus *et al.* reported that CrO_xN_y thin films, prepared by using a metal chromium target with $Ar/O_2/N_2$ gas mixture, exhibited continuous variation of stoichiometry from CrN to Cr_2O_3 by changing the gas composition [28]. Suzuki *et al.* found that the CrO_xN_y films, prepared by pulsed laser deposition using metal Cr targets in ammonia-oxygen or nitrogen-oxygen atmosphere, contained CrN phase with NaCl structure and it increased the hardness of the films when oxygen atoms dissolved in the films [29]. In our previous work [30], we studied the structure and optical properties of a CrO_xN_y film with a wide composition span. In this work, we further study the composition modulation and the relation between bandgap and composition.

In view of the various changes of properties with composition, ~~in this work,~~ we prepared the CrO_xN_y films using the Cr_2O_3 and the CrN compound targets, with N_2 and O_2 reactive gases, respectively. The aim is to fabricate the CrO_xN_y films with adjustable composition and properties. The influence of reactive gases flow rate on the structure, composition and bandgap of the films was investigated. The crystalline structure, composition, and optical transmission and absorption of the films were characterised by X-ray diffraction (XRD), X-ray photoelectron spectroscopy (XPS), and UV-vis-NIR spectroscopy, respectively. The bandgaps of the CrO_xN_y films were deduced from the absorption spectra to obtain the relationship between bandgap and composition.

2. Experimental details

All samples were prepared by RF reactive magnetron sputtering (JCP-500M3 Beijing Techno. Co., Ltd., China) using Cr_2O_3 (99.95%) and CrN (99.95%) stoichiometric compounds as the targets. The substrates were the Si (111), ITO glass, and fused quartz

glasses. Before deposition, the base pressure in the chamber was approximately 6.0×10^{-4} Pa. The working gas was argon (99.999%). The distance from the target to the substrate was about 100 mm. The gases flow rate of N_2 and O_2 (99.999%) was set at 0, 3, 5, 8, 10, 20 sccm and 0, 1, 3, 5 sccm, respectively. Argon gas flow was fixed at a constant flow rate of 50 sccm. In the following, the samples prepared with the Cr_2O_3 target were labeled as Ar=50, N_2:Ar=3:50, N_2:Ar=5:50, N_2:Ar=8:50, N_2:Ar=10:50, N_2:Ar=20:50 and Ar=50, O_2:Ar=1:50, O_2:Ar=3:50, O_2:Ar=5:50 for the CrN target. Before ~~all~~ deposition, the targets were pre-sputtered for 5 minutes to clean the surface. The target RF powers were set at 120 W with a deposition time of 90 min. The thicknesses of the samples prepared with the Cr_2O_3 and CrN targets were in the range of 130~170 nm and 35~60 nm, respectively.

The phase structure of the samples was characterised by XRD using a Bruker D8 Advance X-ray diffractometer in θ-2θ mode with CuKα radiation (0.154 nm). The XPS was used to study the elemental chemical state and composition of the sample using a Thermo Scientific Escalab 250Xi photoelectron spectrometer equipped with an AlK_a X-ray source. The surfaces of all samples were etched and cleaned using argon ions with 2 keV for 180 s or 360 s to check the composition uniformity in depth before measurement. Avantage software was used to analyse the core-level spectra of each element and determine the elemental composition in the samples. The UV-vis-NIR spectroscopy (UV-3600) was used to measure the absorption and transmission of the samples.

3.Results and Discussion

3.1 Phase structure

Figure 1 shows the XRD patterns of the films prepared using the Cr_2O_3 and CrN targets with variation of the N_2 or O_2 flow rate, respectively. As can be seen, the samples show the similar diffraction patterns attributed to almost the same face-centered cubic phase structure. In Figure 1(a), the peak located at 2θ=28.4° is related to Si(111) from the Si substrate. According to standard PDF card (~~PDF~~#43-1040), diffraction peaks located at 2θ=28.6° ~~are~~ correspond to the CrO_2 (110) plane [31]. Additionally, the peaks at 2θ=25.7° and 27.1° probably correspond to Cr_2O_5 (220) and Cr_2O_5 (-221)(~~PDF~~#36-1329), respectively [32]. The intensity of the CrO_2 (110) diffraction peak is the highest, indicating that the film grew preferentially along the CrO_2 (110) plane. Moreover, the variation of the N_2 flow rate brought

no significantly change in CrO_2 and Cr_2O_5 crystallization. Figure 1(b) shows the XRD patterns of the CrO_xN_y films prepared with the use of the CrN target. The chromium oxides as the main phases existed in the samples even prepared without oxygen, which indicates that the CrN was easily oxidized in magnetron sputtering conditions. It is probably due to the presence of residual oxygen adsorbed on the chamber walls.

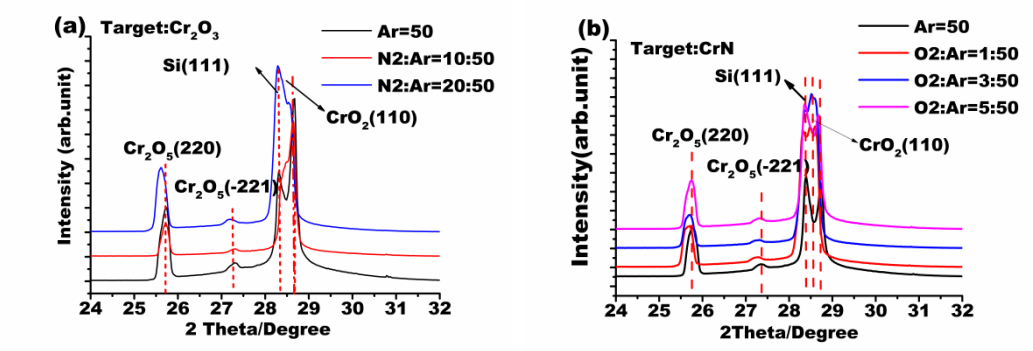

Figure 1. XRD patterns of the CrO_xN_y films prepared with the Cr_2O_3 and the CrN targets by varying N_2 or O_2 gases flow rate. (a) Cr_2O_3 target (b) CrN target.

The XRD results reveal that both groups of samples possessed almost the same phase composition and chromium oxides as main phases. No chromium nitride phase was found in the samples. The probable reason is that it exists in the form of an amorphous phase or in a small amount. A similar result was also reported by Sushant K *et al* [29]. Furthermore, the standard free energy of chromium oxide formation is more negative than that of chromium nitride and therefore the affinity of chromium for oxygen is stronger and ~~it~~ facilitates the formation of chromium oxide [33].

To further observe the structural properties, the Raman spectra of the samples fabricated on the fused quartz substrate are shown in Figure 2. For the samples prepared with the Cr_2O_3 target, they showed similar Raman characteristic peaks different in intensity, as shown in Figure 2(a). The main peaks are located ~~at~~ around 566 cm^{-1} and 1090 cm^{-1}, which ~~are~~ correspond to the characteristic peaks of the CrO_2 [32]. The peak intensity of both peaks increased as the N_2 flow was increased. Meanwhile, the Raman peak positions shift to low wavenumber with N_2 introduction and it is accompanied by significant change of peak shape. The characteristic peaks appeared in the 400-700 cm^{-1} range correspond to both the Cr-N and Cr-O bonds [34]. The weak peak appearing at 775 cm^{-1} comes from the characteristic peak of

the Cr_2O_5 [32]. In addition, the D and G peaks appearing in the N_2:Ar=10:50 and N_2:Ar=20:50 samples are probably due to the organic contamination on the sample surface.

Regarding the samples prepared with the CrN target, the Raman spectra are slightly different from that of the samples prepared with the Cr_2O_3 target. Except for the main Raman peaks at 566 cm^{-1} and 1090 cm^{-1}, two peaks located at 866 cm^{-1} and 1002 cm^{-1} are the characteristic peaks of the Cr_2O_5 and CrO_x [32]. This result indicates the different crystallization qualities of the samples. Furthermore, the intensity of the 866 cm^{-1} Raman peak increases with increasing oxygen flow rate, ~~which was different from~~ unlike that of other peaks.

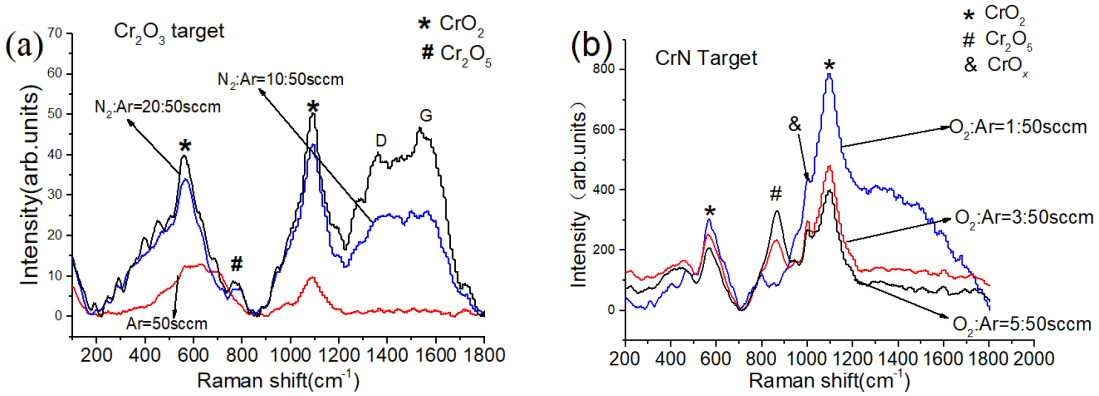

Figure 2. Raman spectra of the samples. (a) Cr_2O_3 target (b) CrN target.

3.2 XPS results of chromium oxynitride films

(1) Elemental composition

Elemental composition of the CrO_xN_y films was deduced from Avantage software by analysing the intensity of the Cr 2p, O 1s and N 1s XPS spectra. Table 1 lists the atomic ratio of the Cr, N, and O elements and the (O+N)/Cr ratio values of all samples. The results show that the nitrogen and oxygen contents in the samples prepared with different targets varied slightly with argon ion etching time.

First, regarding the composition variation of the 180 s samples prepared with the Cr_2O_3 target, oxygen content decreased and nitrogen increased with increase of N_2 gases flow rate. When N_2 gas flow rate increased to 10 sccm and higher, nitrogen and oxygen contents varied significantly. The N/O atomic ratio value was close to 1:1 and 2:1 for the N_2：Ar=10: 50sccm and N_2: Ar=20:50sccm samples, respectively. Furthermore, after the 360 s Ar^+ etching time,

the composition fluctuated slightly with the variation of N_2 gas flow rate.

Table 1. Elemental composition of the chromium oxynitride films.

Target	Reactive gas (sccm)	Ar^+ etching time (s)	Atomic ratio (at. %) (±2.0)			(O+N)/ Cr
			Cr	O	N	
Cr_2O_3	Ar=50	180s	41.2	58.8	--	1.43
	N_2：Ar=3:50		36.5	57.2	6.3	1.74
	N_2：Ar=5:50		36.4	55.7	7.9	1.75
	N_2：Ar=8:50		37.2	55.9	6.9	1.69
	N_2：Ar=10:50		39.2	30.2	30.6	1.55
	N_2：Ar=20:50		35.4	21.8	43.0	1.83
	Ar=50	360s	41.3	58.7	--	1.42
	N_2：Ar=3:50		37.8	54.9	7.3	1.65
	N_2：Ar=5:50		35.9	57.6	6.5	1.79
	N_2：Ar=8:50		37.1	56.3	6.6	1.69
	N_2：Ar=10:50		41.5	31.4	27.1	1.41
	N_2：Ar=20:50		36.7	17.7	45.6	1.72
CrN	Ar=50	180s	56.1	20.2	23.1	0.77
	O_2：Ar=1:50		39.2	61.3	--	1.56
	O_2：Ar=3:50		37.9	62.1	--	1.64
	O_2：Ar=5:50		37.7	62.3	--	1.65
	Ar=50	360s	50.2	19.1	21.2	0.80
	O_2：Ar=1:50		38.9	61.1	--	1.68
	O_2：Ar=3:50		36.7	63.3	--	1.75
	O_2：Ar=5:50		36.3	63.7	--	1.77

Regarding the samples prepared with the CrN target, the introduction of a small amount of O_2 resulted in the loss of nitrogen in the sample. Oxygen atoms always existed in the samples even without O_2 introduction. This once again indicates that the CrN target was

easily oxidized under sputtering, and that the oxygen probably mainly came from residual atmosphere in the chamber or from adsorbed oxygen on the chamber wall.

The non-metal to metal (O+N)/Cr ratio values were calculated and ~~they~~ show a fluctuation with reactive gas flow rate for the samples prepared using 360 s and 180 s Ar^+ etching times. The (O+N)/Cr ratio values were in the range of 1.42~1.83 and 0.77~1.77 in the samples prepared with the Cr_2O_3 and CrN targets, respectively. When the N_2 flow rate was set at 3, 5, 8 sccm, the N and O compositions in the film did not have significant changes. Once the nitrogen flow rate was increased up to 10 sccm or higher, the N and O concentrations significantly changed. Regarding the samples prepared with the CrN target, nitrogen almost disappeared once O_2 gases were introduced. It means that most of the oxygen atoms replaced the nitrogen atoms during growth and chromium oxides were formed.

3.3 Chemical bond state analysis

(1) Fitting of XPS spectra of samples

To further analyse the chemical bond state in the samples, we performed the decomposition of the XPS spectra recorded after surface argon ion etching for 360 s. The decompositions of the Cr 2p, N 1s and O 1s core-level spectra are shown in Figure 3. When the N_2 flow rate was set at 10 sccm and higher, the core-level spectra had significant changes. Therefore, here, we analysed the Cr 2p, N 1s and O 1s core-level spectra of the Ar=50, N_2:Ar=10:50, N_2:Ar=20:50 samples. Figure 3(a) presents the fitting of the Cr 2p spectra decomposed with three doublets. The O 1s spectra, as shown in Figure 3(b), consisted of two components for the Ar=50 and N_2:Ar=10:50 samples, but three components are needed for the N_2:Ar=20:50 sample. The fitting of the N 1s spectra, as shown in Figure 3(c), presented different components, two for the Ar=50 sample and three for the N_2:Ar=10:50 and N_2:Ar=20:50 samples.

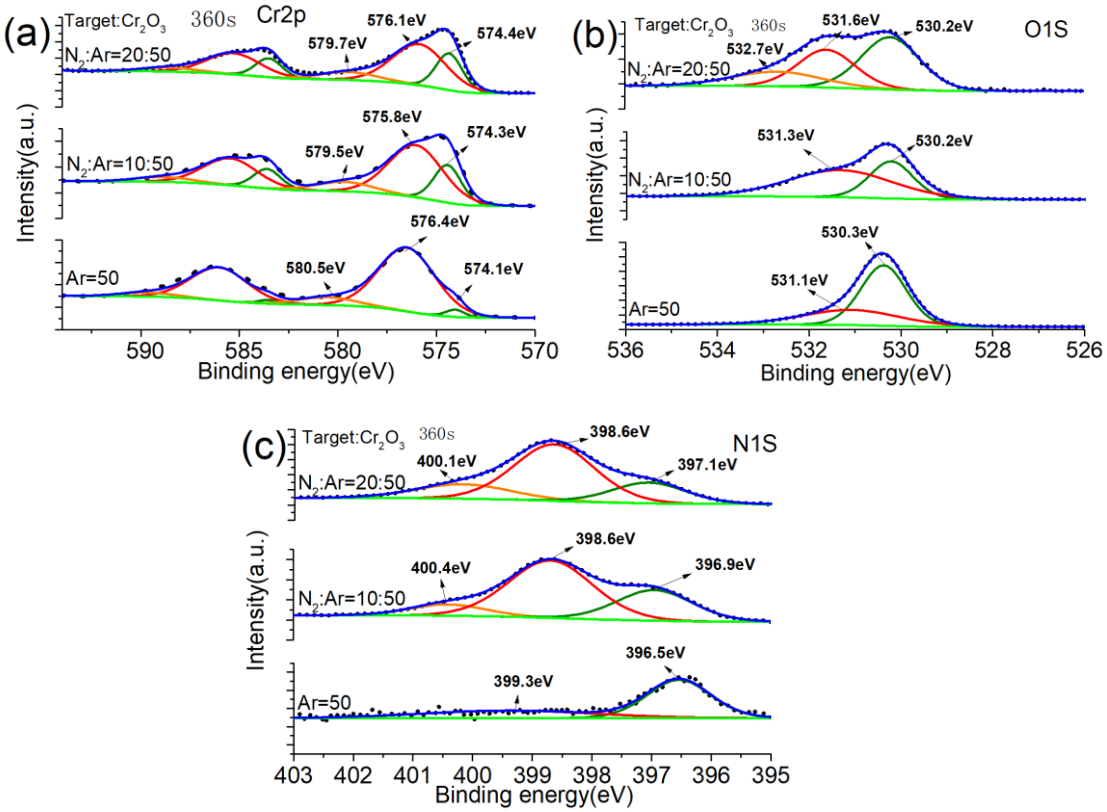

Figure 3. Fitting of XPS spectra of the samples prepared with the Cr_2O_3 target with varied N_2 flow rates. (a) Cr2p (b) O1s (c) N1s.

As the Cr 2p spectra were a doublet peak we only discussed the Cr $2p_{3/2}$ peak. For the N_2:Ar=20:50 sample, the binding energies of the three components were located at 574.4, 576.1 and 579.7 eV. The 574.4 eV binding energy corresponded to the Cr-N bond and 576.1 eV and 579.7 eV to the Cr-O bond of the CrO_2 and CrO_3 compounds, respectively [35, 36]. For the two other samples, there was a slight shift in peaks compared with that of the N_2:Ar=20:50 sample. Therefore, the chemical state in three samples was similar but the relative intensities of the three components varied with the reactive gas flow rate. Therefore, we analysed the integral area of the fitting components for the three samples. The integral area of the 574.4 eV component gradually increased with increased nitrogen flow rate, indicating the increase in the number of the Cr-N bonds. The integral areas of the components located at 576.1 and 579.7 eV gradually decreased, indicating a decrease in the number of the Cr-O bonds. That is to say, the increase in the number of the Cr-N bonds accompanied with a decrease in the number of the Cr-O bonds.

Figure 3(b) shows the O 1s spectra. Regarding the sample N_2:Ar=20:50, the O 1s spectrum consisted of three components located at 530.2, 531.6 and 532.7 eV. The 530.2 eV

binding energy corresponded to the Cr-O bond of the CrO_3 compound. The 531.6 and 532.7 eV binding energies corresponded to the Cr^{3+} and Cr^{4+} states in the CrO_x compound. The areas of the two main components, 530.2 and 531.6 eV, decreased with increased nitrogen flow rate, indicating a decrease in the number of the Cr-O bonds.

Figure 3(c) gives the fittings of the N 1s spectra. For the N_2:Ar=20:50 sample, the peak consisted of three components with binding energies located at 397.1, 398.6, and 400.1 eV. The 397.1 and 398.6 eV binding energies corresponded to the Cr-N bond in CrN_x compound [35]. The component at 400.1 eV corresponds to the N-O bonds. The integral area of the 397.1 eV peak first increased and then decreased slightly with increased nitrogen flow rate. The integral area of the component at 398.6 eV increased significantly.

Figure 4 shows the fittings of the Cr 2p, O 1s and N 1s core-level spectra of the four samples prepared at Ar=50, O_2:Ar=1:50, O_2:Ar=3:50 and O_2:Ar=5:50 sccm. The samples obtained with and without oxygen introduction showed a significant change in peak positions and peak shapes. It is obviously to see that only the Ar=50 sample presented the N 1s peaks.

The Cr $2p_{3/2}$ peaks composed of three components located at 573.9, 575.1, and 578.2 eV, as shown in Figure 4(a). The 573.9 eV peak corresponds to the Cr-N bonds in the CrN_x compound. The components at 575.1 and 578.2 eV correspond to the Cr-O bonds in the CrO_2 and CrO_3 compounds, respectively. For the O_2:Ar=1:50 sample , the binding energies of the three components are located at 576.3eV, 577.8eV and 582.4eV, corresponding to the Cr-O bond in intermediate oxide CrO_x. The other two samples prepared with oxygen introduction showed a small peak shift compared to the O_2:Ar=1:50 sample. Therefore, they had almost the same chemical bond state, but a variation of chemical bond proportions. Compared with the integral area of each component peak in the four samples, the component at 573.9 eV decreased dramatically when O_2 gas was introduced. Meanwhile the increase of the area of the two components area at 575.1 and 578.2 eV indicates the increase in the proportion of the Cr-O bonds with the oxygen flow rate.

Figures 4(b) and (c) show the fittings of the O 1s and N 1s spectra, respectively. For the Ar=50 sample, the O 1s peak consists of two components located at 530.5 and 532.2 eV, which correspond to the Cr-O and OH species, respectively. The other samples had similar results. With respect to the integral area of each component, the Cr-O bond proportion increased with the O_2 gases flow rate. The N 1s peak composed of two components with binding energies located at 397.1 and 398.2 eV, which correspond to the Cr-N bonds in CrN_x compounds.

It is known that in the XRD results there was no CrN_x phases detected. However, the

Cr-N bonds were founded in the XPS analysis. The probable reasons attributed to the presence of the amorphous CrN_x phase or solid solution CrO_xN_y in the samples.

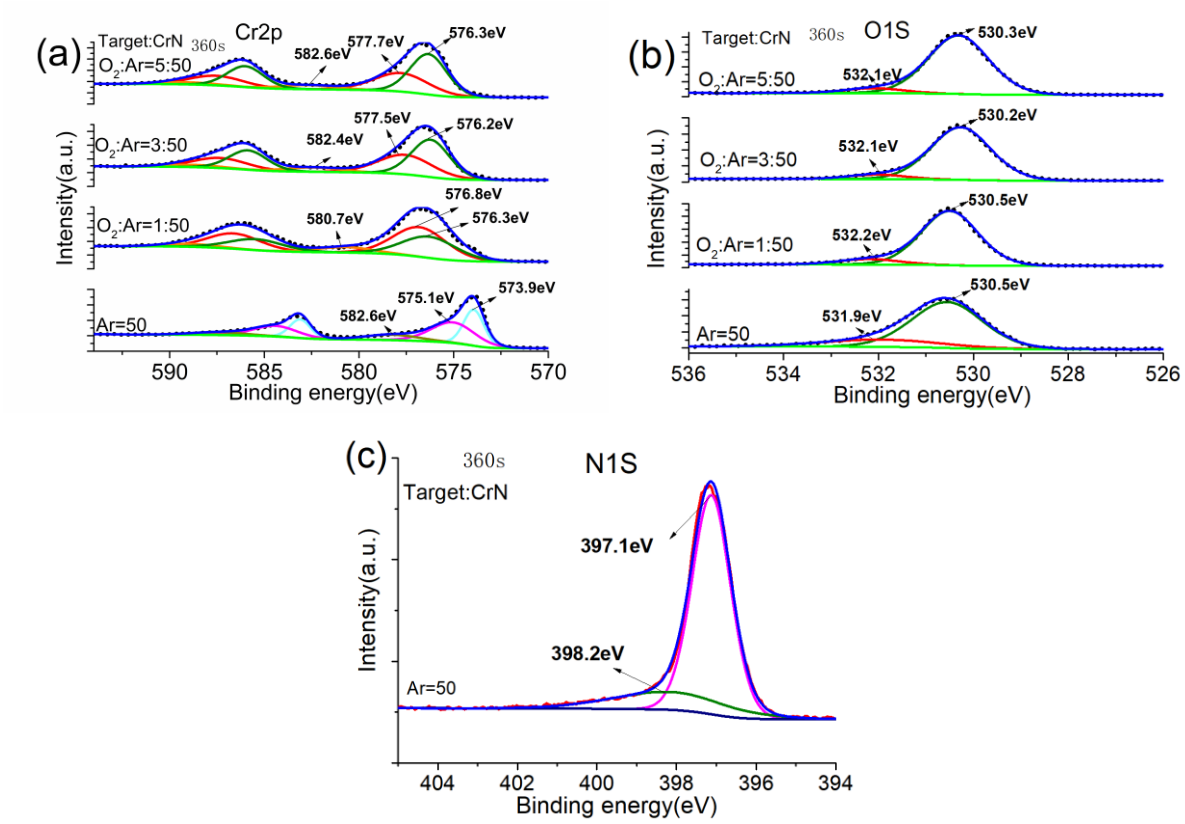

Figure 4. XPS fitting results of the samples prepared with the CrN target with various of O_2 flow rate. (a) Cr2p (b) O1s (c) N1s.

3.4 Optical properties

Figures 5(a) and (b) show the transmission of the samples deposited on the ITO glass and quartz substrates, respectively. The transmission of the samples on the ITO glass increased with an increase of O_2 flow rate from 65 to 90% in the range of 500~1200 nm. The maximum value was approximately 90% for the N_2:Ar=10:50 sample. In the 400~500 nm range, the transmission values increased with wavelength. Regarding the samples on the quartz substrate, the transmission maximum value was approximately 85% for the N_2:Ar=20:50 sample. The transmission values of the Ar=50 sample was lower than that of other samples. We further compared the absorption value of the samples on quartz, as shown in Figure 5(c). All samples had a low absorption value equal to approximately 0.2. The absorption edge of the Ar=50 sample significantly differed from that of other samples. This

result indicates that the samples prepared with introduction of N_2 gases shown a significantly absorption edge shift towards shorter wavelengths.

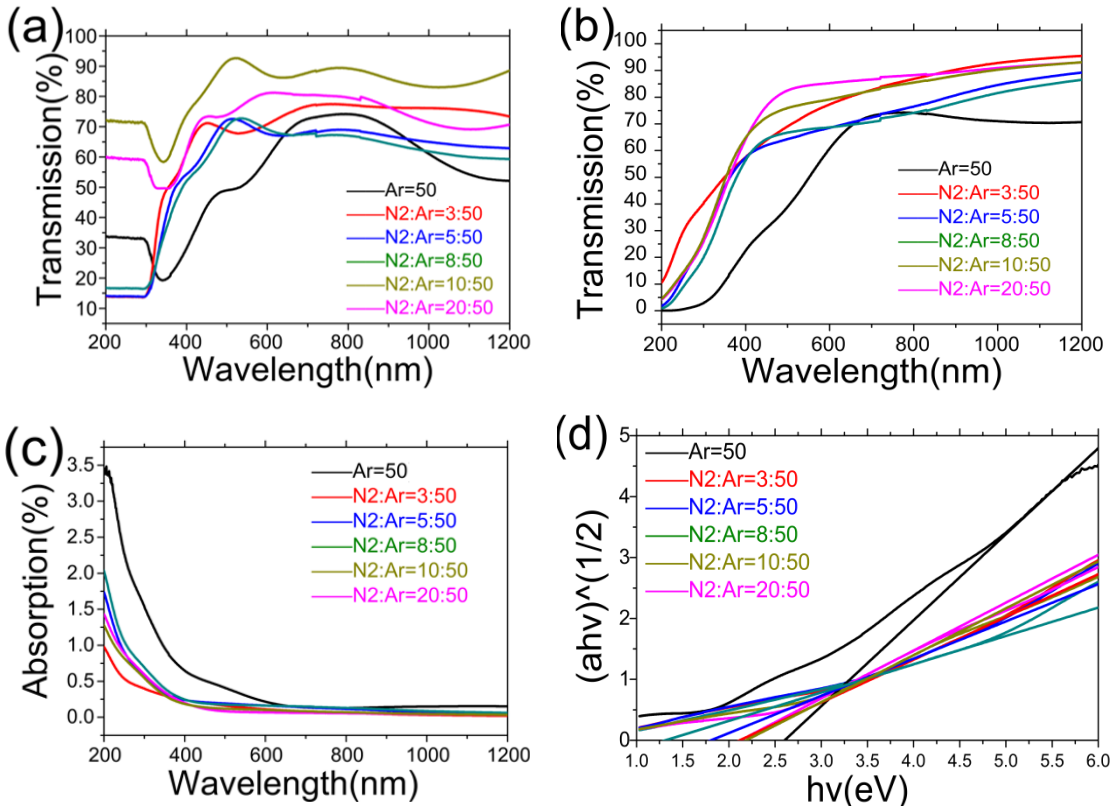

Figure 5. Optical properties of the CrO_xN_y films prepared with the Cr_2O_3 target on the ITO-glass and the quartz substrates. (a) transmission of the films on the ITO glass (b) transmission of the films on the quartz substrate (c) absorption of the films on the quartz substrate (d) $(\alpha hv)^{1/2}$ & hv curves.

To determine the bandgap of the chromium oxynitride films, the bandgap values of the films were deduced from the absorption spectra using the following Tauc relationship [37]

$$(\alpha hv / A)^{1/2} = hv - E_g \qquad (3\text{-}1)$$

where h is Planck's constant, v is the light frequency, E_g is the bandgap, α is the absorption coefficient and A is a constant. We plotted the curve using $(\alpha hv)^{1/2}$ as the y-axis and hv as the x-axis and then made a linear fitting [38-40]. The bandgap values were determined from the intercept of the linear fitting at the origin of the y-axis, where E_g is equal to hv, as shown in Figure 5(d). The deduced E_g values of the samples prepared

using the Cr_2O_3 target lied in the range of 1.4~2.6 eV.

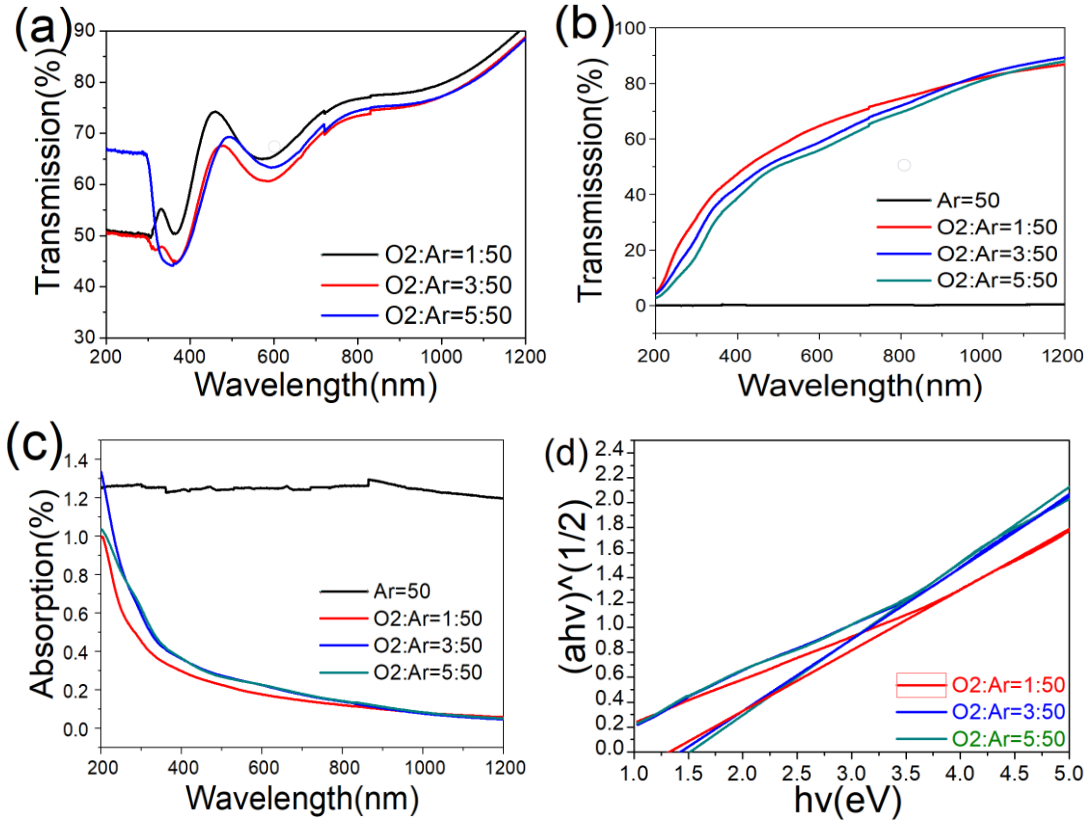

Figure 6. Optical properties of the CrO_xN_y films prepared with CrN target. (a): transmission of the films on the ITO glass substrate (b): transmission of the films on the quartz substrate (c): absorption of the films on the quartz substrate (d) $(\alpha hv)^{1/2}$ & hv curves.

Figure 6 shows optical properties of the CrO_xN_y films prepared with the CrN target on the ITO glass and quartz substrates. Regarding the films on the ITO glass shown in Figure 6(a), the three samples showed the similar transmission values in the visible range. At the wavelength of 380 nm, a significant increase of transmission up to 65% occurs and it is followed by a decrease to 60% at 600 nm and then a slight rise. For the films on the fused quartz substrates, the transmission of the samples with O_2 introduction increased gradually with wavelength, as shown in Figure 6(b), and show a significant difference with that of the sample without O_2 introduction. This indicates that the introduction of O_2 brought a significantly composition change in the sample.

Figures 6(c) and (d) show the absorption value and the deduced $(\alpha hv)^{1/2}$ & hv curves of the samples. The samples without O_2 introduction showed a higher absorption over whole

measured wavelength range. After O_2 introduction, the absorption significantly decreased. The absorption edge of the three samples with O_2 introduction showed a slight difference. According to Tauc relationship [30], the deduced bandgap values from absorption spectra were 1.3, 1.4, and 1.5 eV for the O_2:Ar=1:50, O_2:Ar=3:50, O_2:Ar=5:50 samples, respectively.

4. Conclusions

Structure, composition, and optical properties of the CrO_xN_y films prepared by reactive magnetron sputtering were studied. XRD results showed that the main phase present in the samples was mainly CrO_2 with a CrO_2 (110) preferential orientation. The XPS results indicated that in the samples prepared with the Cr_2O_3 target, the Cr-N bond content increased with the increase of N_2 flow rate and it was accompanied with a decrease of the Cr-O bond content. This result indicated that nitrogen atoms were gradually incorporated into the samples and replaced a part of oxygen atoms. Therefore, the samples prepared with the Cr_2O_3 target and N_2 gas realized composition modulation to some extent. The Cr-O bonds mainly presented in the samples prepared with the CrN target and no Cr-N bonds were observed. It indicated that it is difficult to modulate film composition using the CrN target with various O_2. The samples prepared with both targets possessed good transmission in visible and NIR range. According to the absorption spectra, the deduced bandgap varied over 1.3~2.6 eV.

Acknowledgements

The authors thank the support of the National Natural Science Foundation of China (Project No. 51702133). We are also thankful for the support of Postgraduate Research & Practice Innovation Program of Jiangsu Province (No. KYCX20_3129).

References

[1] E. Carretero, R. Alonso, C. Pelayo, Optical and electrical properties of stainless steel oxynitride thin films deposited in an in-line sputtering system, Applied Surface Science,379 (2016) 249–258.

[2] S.T. Oyama, Introduction to the chemistry of transition metal carbides and nitrides, 1996.

[3] C.T. Campbell, Transition metal oxides: extra thermodynamic stability as thin films, Phys Rev Lett, 96 (2006) 066106.

[4] C.V. Ramana, V.V. Atuchin, L.D. Pokrovsky, U. Becker, C.M. Julien, Structure and chemical properties of molybdenum oxide thin films, Journal of Vacuum Science & Technology A: Vacuum, Surfaces, and Films, 25 (2007) 1166-1171.

[5] P. Ashrit, Introduction to Transition Metal Oxides and Thin Films, Transition Metal Oxide Thin Film based Chromogenics and Devices, 2017, 13-72.

[6] V.N. Kruchinin, T.V. Perevalov, V.V. Atuchin, V.A. Gritsenko, A.I. Komonov, I.V. Korolkov, L.D. Pokrovsky, C.W. Shih, A. Chin, Optical Properties of TiO_2 Films Deposited by Reactive Electron Beam Sputtering, Journal of Electronic Materials, 2017, 46: 6089-6095.

[7] V.V. Atuchin, M.S. Lebedev, I.V. Korolkov, V.N. Kruchinin, E.A. Maksimovskii, S.V. Trubin, Composition-sensitive growth kinetics and dispersive optical properties of thin $Hf_xTi_{1-x}O_2$ $(0 \leq x \leq 1)$ films prepared by the ALD method, Journal of Materials Science: Materials in Electronics, 2018, 30:812-823.

[8] V. Garg, B.S. Sengar, V. Awasthi, A. Kumar, R. Singh, S. Kumar, C. Mukherjee, V.V. Atuchin, S. Mukherjee, Investigation of Dual-Ion Beam Sputter-Instigated Plasmon Generation in TCOs: A Case Study of GZO, ACS Appl Mater Interfaces, 10 (2018) 5464-5474.

[9] S. Zheng, W. Li, T. Su, F. Xie, J. Chen, Z. Yang, Y. Zhang, S. Liu, M.P. Aldred, K.Y. Wong, J. Xu, Z. Chi, Metal Oxide CrOx as a Promising Bilayer Electron Transport Material for Enhancing the Performance Stability of Planar Perovskite Solar Cells, Solar RRL, 2 (2018).

[10] L. Yu, J. Chen, H. Ju, H. Dong, H. Zhao, Influence of Al content on microstructure, mechanical and tribological properties of Ti-W-Al-N composite films, Vacuum, 137 (2017) 31-37.

[11] H. Ju, J. Xu, Influence of vanadium incorporation on the microstructure, mechanical and tribological properties of Nb–V–Si–N films deposited by reactive magnetron sputtering, Materials Characterization, 107 (2015) 411-418.

[12] J. Xu, H. Ju, L. Yu, Microstructure, oxidation resistance, mechanical and tribological properties of Mo–Al–N films by reactive magnetron sputtering, Vacuum, 103 (2014) 21-27.

[13] J. Xu, H. Ju, L. Yu, Influence of silicon content on the microstructure, mechanical and tribological properties of magnetron sputtered Ti–Mo–Si–N films, Vacuum, 110 (2014) 47-53.

[14] V.V. Atuchin, V.N. Kruchinin, A.V. Kalinkin, V.S. Aliev, S.V. Rykhlitskiĭ, V.A. Shvets, E.V. Spesivtsev, Optical properties of the $HfO_{2-x}N_x$ and TiO_{2-x} N_x films prepared by ion beam sputtering, Optics and Spectroscopy, 106 (2009) 72-77.

[15] A.M. Abd El-Rahman, S.H. Mohamed, Preparation and characterization of nanostructured titanium oxynitride films for the application in self-cleaning and photoelectrochemical water splitting, Thin Solid Films, 698 (2020).

[16] P. Khwansungnoen, S. Chaiyakun, T. Rattana, Room temperature sputtered titanium oxynitride thin films: The influence of oxygen addition, Thin Solid Films, 711 (2020).

[17] Y.H. Wong, V.V. Atuchin, V.N. Kruchinin, K.Y. Cheong, Physical and dispersive optical characteristics of ZrON/Si thin-film system, Applied Physics A, 115 (2013) 1069-1072.

[18] G.I. Cubillos, M.E. Mendoza, J.E. Alfonso, G. Blanco, M. Bethencourt, Chemical composition and microstructure of zirconium oxynitride thin layers from the surface to the substrate-coating interface, Materials Characterization, 131 (2017) 450-458.

[19] C.I. da Silva Oliveira, D. Martinez-Martinez, L. Cunha, M.S. Rodrigues, J. Borges, C. Lopes, E. Alves, N.P. Barradas, M. Apreutesei, Zr-O-N coatings for decorative purposes: Study of the system stability by exploration of the deposition parameter space, Surface and Coatings Technology, 343 (2018) 30-37.

[20] D. Cristea, A. Crisan, D. Munteanu, M. Apreutesei, M.F. Costa, L. Cunha, Tantalum oxynitride thin films: Mechanical properties and wear behavior dependence on growth conditions, Surface and Coatings Technology, 258 (2014) 587-596.

[21] H. Le Dréo, O. Banakh, H. Keppner, P.A. Steinmann, D. Briand, N.F. de Rooij, Optical, electrical and mechanical properties of the tantalum oxynitride thin films deposited by pulsing reactive gas sputtering, Thin Solid Films, 515 (2006) 952-956.

[22] J. Hirpara, V. Chawla, R. Chandra, Investigation of tantalum oxynitride for hard and anti-corrosive coating application in diluted hydrochloric acid solutions, Materials Today Communications, 23 (2020).

[23] P. Carvalho, J. Borges, M.S. Rodrigues, N.P. Barradas, E. Alves, J.P. Espinós, A.R. González-Elipe, L. Cunha, L. Marques, M.I. Vasilevskiy, F. Vaz, Optical properties of zirconium oxynitride films: The effect of composition, electronic and crystalline structures, Applied Surface Science, 358 (2015) 660-669.

[24] U.N. Kumar, J.N. Ramavath, S. Ghosh, R. Kothandaraman, T. Thomas, Chromium Oxynitride as Durable Electrode Material for Symmetric Supercapacitors, Batteries & Supercaps, 3 (2020) 780-788.

[25] E. Martinez, R. Sanjinés, O. Banakh, F. Lévy, Electrical, optical and mechanical properties of sputtered CrN_y and $Cr_{1-x}Si_xN_{1.02}$ thin films, Thin Solid Films, 447-448 (2004) 332-336.

[26] R. Arvinte, J. Borges, R.E. Sousa, D. Munteanu, N.P. Barradas, E. Alves, F. Vaz, L. Marques, Preparation and characterization of CrN_xO_y thin films: The effect of composition and structural features on the electrical behavior, Applied Surface Science, 257 (2011) 9120-9124.

[27] S.K. Rawal, A.K. Chawla, R. Jayaganthan, R. Chandra, Optical and hydrophobic properties of co-sputtered chromium and titanium oxynitride films, Applied Surface Science, 257 (2011) 8755-8761.

[28] R. Mientus, R. Grötschel, K. Ellmer, Optical and electronic properties of CrO_xN_y films, deposited by reactive DC magnetron sputtering in $Ar/N_2/O_2(N_2O)$ atmospheres, Surface and Coatings Technology, 200 (2005) 341-345.

[29] T. Suzuki, J. Inoue, H. Saito, M. Hirai, H. Suematsu, W. Jiang, K. Yatsui, Influence of oxygen content on structure and hardness of Cr–N–O thin films prepared by pulsed laser deposition, Thin Solid Films, 515 (2006) 2161-2166.

[30] Y.Y. Yuan, B.Y. Zhang, J. Sun, P. Jonnard, K. Le Guen, Y.C. Tu, C. Yan, R. Lan, Structure and optical properties of CrO_xN_y films with composition modulation, Surf. Eng., 36 (2019) 411-417.

[31] K. Suzuki, P.M. Tedrow, Selective deposition of CrO_2 films on glass substrates, Solid State Communications, 107 (1998) 583-585.

[32] L.T. O. Monnereau, C. E. A. Grigorescu, D. Savastru, C.R.I. , F.G. , R. Notonier, A.T. , T.Z. , I.N.M. , D.S. , H.J.T. , Chromium oxides mixtures in PLD films investigated by Raman spectroscopy, Journal of optoelectronics and advanced materials, 12 (2010) 1752-1758.

[33] T. Minami, S. Nishio, Y. Murata, Periodic microstructures of Cr–O–N coatings deposited by arc ion plating, Surface and Coatings Technology, 254 (2014) 402-409.

[34] Z.B. Qi, B. Liu, Z.T. Wu, F.P. Zhu, Z.C. Wang, C.H. Wu, A comparative study of the oxidation behavior of Cr2N and CrN coatings, Thin Solid Films, 544 (2013) 515-520.

[35] A. Vyas, Z.F. Zhou, Y.G. Shen, Effect of aluminum contents on sputter deposited CrAlN thin films, IOP Conference Series: Materials Science and Engineering, 307 (2018).

[36] https://srdata.nist.gov/xps/Default.aspx.

[37] J. Tauc, Amorphous and Liquid Semiconductor, Plenium Press, NewYork, 1974.

[38] C.V. Ramana, G. Carbajal-Franco, R.S. Vemuri, I.B. Troitskaia, S.A. Gromilov, V.V. Atuchin, Optical properties and thermal stability of germanium oxide (GeO_2) nanocrystals with α-quartz structure, Materials Science and Engineering: B, 174 (2010) 279-284.

[39] V.V. Atuchin, L.I. Isaenko, V.G. Kesler, Z.S. Lin, M.S. Molokeev, A.P. Yelisseyev, S.A. Zhurkov, Exploration on anion ordering, optical properties and electronic structure in K3WO3F3 elpasolite, Journal of Solid State Chemistry, 187 (2012) 159-164.

[40] H. Ji, Z. Huang, Z. Xia, M.S. Molokeev, X. Jiang, Z. Lin, V.V. Atuchin, Comparative investigations of the crystal structure and photoluminescence property of eulytite-type Ba3Eu(PO4)3 and Sr3Eu(PO4)3, Dalton Trans, 44 (2015) 7679-7686.